Interface disorder probed at the atomic scale for graphene grown on the C face of SiC

G. Nicotra,[1] I. Deretzis,[1] M. Scuderi,[1] C. Spinella,[1] P. Longo,[2] R. Yakimova,[3] F. Giannazzo,[1] and A. La Magna[1,*]

[1]*Istituto per la Microelettronica e Microsistemi (CNR-IMM), VIII Strada 5, I-95121 Catania, Italy*

[2]*Gatan, Inc., 5794 West Las Positas Boulevard, Pleasanton, California 94588, USA*

[3]*Department of Physics, Chemistry and Biology, IFM, Linköping University, SE-581 83 Linköping, Sweden*

(Received 11 December 2014; revised manuscript received 13 March 2015; published 10 April 2015)

We use aberration-corrected scanning transmission electron microscopy, electron energy-loss spectroscopy, atomic force microscopy, and the density functional theory to study the structural and electronic characteristics of graphene grown on the C face of SiC. We show that for high growth temperatures the graphene/SiC(000$\bar{1}$) interface is dominated by a thin amorphous film which strongly suppresses the epitaxy of graphene on the SiC substrate. This film maintains an almost fixed thickness regardless of the number of the overlying graphene layers, while its chemical signature shows the presence of C, Si, and O. Structurally, the amorphous area is inhomogeneous, as its Si concentration gradually decreases while approaching the first graphene layer, which is purely sp^2 hybridized. *Ab initio* calculations show that the evaporation process and the creation of Si vacancies on the C face of SiC strongly enhance the surface disorder and designate defect areas as preferential sublimation sites. Based on these features, we discuss differences and similarities between the C-only buffer layer that forms on the Si face of SiC and the thicker C-Si-O amorphous film of the C face.

DOI: 10.1103/PhysRevB.91.155411 PACS number(s): 81.05.ue, 73.22.Pr, 68.37.Nq

I. INTRODUCTION

The precise control over the graphitization of SiC surfaces is a key step for the production of large-scale epitaxial graphene films. Such control has been widely achieved for graphene grown on the Si face of SiC, where single-crystalline, homogeneous, and continuous monolayers can cover entire areas from the micro- to the milliscale [1–4]. On the other hand, even under similar growth conditions, graphitization over the C face of SiC is still challenging. Graphene on the (000$\bar{1}$) plane shows structural and electronic inhomogeneity [2,5,6], which affects the number of graphene layers, their orientation, the stacking order, and doping concentration. Notwithstanding the presence of this apparent disorder, graphene on the C face still remains technologically appealing, as measured mobilities outscore those of the Si face [7,8], rendering it an extremely important material for next-generation electronics.

The origin of the differences in the morphological and electrical properties of samples grown on the two polar SiC{0001} surfaces (i.e., the Si face and the C face) is still a matter of debate. A starting point for understanding this critical issue is the morphology of the graphene/SiC interface. At the Si face, a well defined interface structure has been identified by means of both experimental [9–12] and theoretical studies [13,14], which is thought to influence both the epitaxial process as well as the electrical characteristics [15] of the overlying graphene. This so-called buffer layer has a $(6\sqrt{3} \times 6\sqrt{3})R30^\circ$ periodicity with respect to the SiC(0001) surface and it consists of a single but corrugated layer of C atoms arranged in a honeycomb structure with a mixed sp^2-sp^3 hybridization (where the sp^3 bonds are the signature of a covalent binding with the Si-terminated surface). The picture is not equally clear for graphene grown on the C face. Apart from a general acceptance of a weaker interface coupling with respect to the Si face [16,17], uncertainty still exists on whether graphene grows directly on the C-terminated surface [18,19] or if it is preceded by either ordered surface reconstructions [16] or a disordered/amorphous interface layer [20–22]. Further dispute exists on whether the formation of graphene on the C face is driven by an epitaxial process, as the presence of domains with different orientations and numbers of graphene layers indicates the possible suppression of related mechanisms. We note here that Si-face graphene is clearly epitaxial with a single orientation with respect to the SiC substrate.

The present paper intends to contribute to this debate by means of atomic-resolution imaging and spectroscopic techniques that have not been previously used for the study of graphene grown on the C face of SiC [i.e., low-energy aberration-corrected scanning transmission electron microscopy (STEM) together with atomic-resolution electron energy-loss spectroscopy (EELS)]. In accordance with previous studies [20–22], we show that within the growth conditions of our sample (T=1900 °C in an Ar environment) an amorphous interface film forms at the interface between graphene and SiC. In addition, our analysis demonstrates that this amorphous layer is not homogeneous, as its silicon concentration gradually decreases while moving from its substrate-looking side toward graphene. Moreover, a partial oxidation is chemically detected, which is strictly confined within this amorphous region. The quasifixed thickness of this film as well as its presence throughout the sample, independently from the number of the overlying graphene layers, give strong evidence for the suppression of epitaxial processes in our C-terminated system.

The paper is organized as follows: Sec. II gives experimental details on sample preparation and characterization as well as calculation details, Sec. III discusses planar and cross-sectional morphological characteristics, Sec. IV analyzes the chemical and electronic properties of the graphene/SiC(000$\bar{1}$) heterojunction, Sec. V shows calculation estimates of the structural modifications in both Si- and C-face SiC when creating Si vacancies, while in Sec. VI we discuss our results.

*antonino.lamagna@imm.cnr.it

II. METHODS

A. Experimental

Graphene growth was carried out by the thermal annealing of a nominally on-axis 4H-SiC(000$\bar{1}$) substrate at a temperature of 1900 °C in an inert gas (Ar) atmosphere with an atmospheric pressure of 1 atm [6]. The morphological properties were studied with atomic force microscopy (AFM) measurements, performed with a DI3100 microscope supplied by Veeco with Nanoscope V electronics. Topography and phase images were measured in tapping mode, using Si probes with ∼10-nm curvature radius and with ∼360-kHz cantilever resonance frequency. After the AFM characterization, samples were prepared in cross section for the STEM analysis by a mechanical thinning followed by low-energy ion milling (3 keV). The incidence angle for the ion guns was always kept below 8° in a single-side mode, i.e., with the ion guns sputtering from the SiC bulk side, in order to avoid direct ion hitting of the graphene surface. We finalized the polishing by lowering the incidence angle down to 3°, in order to reduce the background noise ratio of the images. All STEM and atomic EELS measurements were performed using our sub-Angstrom aberration-corrected JEOL ARM200F microscope, which consists of a probe corrected STEM microscope equipped with a C-FEG and a fully loaded GIF Quantum ER as EELS spectrometer. Our study was performed at the so-called gentle STEM condition [23] at 60-keV primary beam energy. This condition ensured no damage for our samples during STEM and EELS acquisition, as the knock-on threshold for carbon is ∼85 keV, well above the operated energy of this study. This particular installation delivered a probe size of 1.1 Å at 60 keV. Low- and core-loss spectra were nearly simultaneously acquired using the dual EELS capability. The area in the TEM sample used for the EELS investigation was relatively thick (∼1.2t/λ with t the thickness of the lamella and λ the electron mean free path). The presence of the low-loss spectrum allowed for removing the effects of plural scattering that blur the shape of the near edge structure by means of Fourier ratio deconvolution. Low- and core-loss EELS spectra were taken by scanning the electron beam across the interface in the high-angle annular dark field (HAADF) STEM image shown Fig. 3 while moving from the SiC substrate toward the graphene layers. The total exposure time for acquiring the entire EELS spectra data cube was less than 2 min. The spectrometer was set to 0.25-eV dispersion yielding 0.75-eV energy resolution. Such energy resolution is sufficient to reveal different features in the fine structure of the C-K edge and Si-L_1 and -$L_{2,3}$ edges.

B. Theoretical

In order to understand the structural dynamics that emerge during the sublimation process, we modeled 4 × 4 supercells of 4H-SiC slabs with Si vacancies for both Si- and C-terminated surfaces. The 4H-SiC models were composed of four bilayers of SiC passivated with H at the lower termination of the slab, whereas defects were included on the top bilayer. Density functional theory (DFT) calculations were performed with the SIESTA code [24], within the framework of the local density approximation [25]. The wave functions were constructed on a basis set of double-ζ plus polarization orbitals

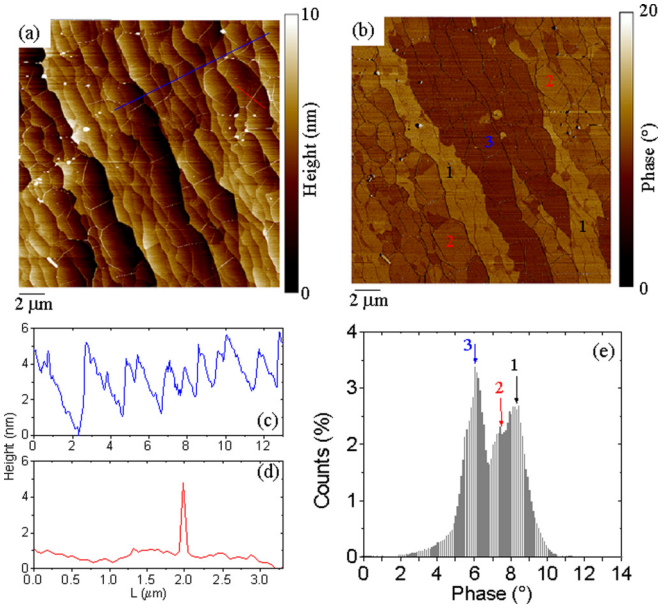

FIG. 1. (Color online) AFM morphology (a) and phase images (b) of the graphene/SiC(000$\bar{1}$) surface. Typical height line profiles of the stepped SiC surface (c) and of a graphene wrinkle (d). Histogram of the values extracted from the phase image (e). The three main peaks in this phase value distribution (indicated by vertical arrows) correspond to surface areas with a different number of graphene layers.

for all elements. Troulier-Martins pseudopotentials [26] were employed for the modeling of ionic cores. Convergence was achieved with a Brillouin-zone sampling based on a 3 × 3 × 1 Monkhorst-Pack grid [27]. A mesh cutoff energy of 280 Ry was set for real-space integration, while structures were relaxed with a force minimization criterion of 0.04 eV/Å.

III. STRUCTURAL AND MORPHOLOGICAL ANALYSIS

After growth, the surface morphology and the graphene coverage uniformity were preliminarily characterized by AFM measurements in tapping mode. Figures 1(a) and 1(b) show typical topographical and phase images of graphene grown on SiC(000$\bar{1}$) at 1900 °C in an Ar atmosphere. As a result of the high-temperature thermal treatment, the SiC surface exhibits micrometer wide terraces and few nanometer high steps, as shown in the height line profile in Fig. 1(c). Furthermore, a net of wrinkles, i.e., peculiar corrugations of the graphene membrane, is superimposed to the stepped SiC surface. These corrugations originate from the compressive stress on the graphene membrane during the cooling down step of the growth process, due to the thermal expansion coefficient mismatch between graphene and SiC. The height of these features can range from ∼1 to ∼4 nm [see the line profile of Fig. 1(d)]. Since wrinkles represent a clear signature of graphene formation, the absence of these features in some regions of Fig. 1(a) indicates an incomplete graphene coverage of the SiC surface. Additional information on the lateral uniformity of graphene can be obtained from the phase image in Fig. 1(b). The variable contrast in the phase image originates from the different electrostatic force gradients experienced by the oscillating

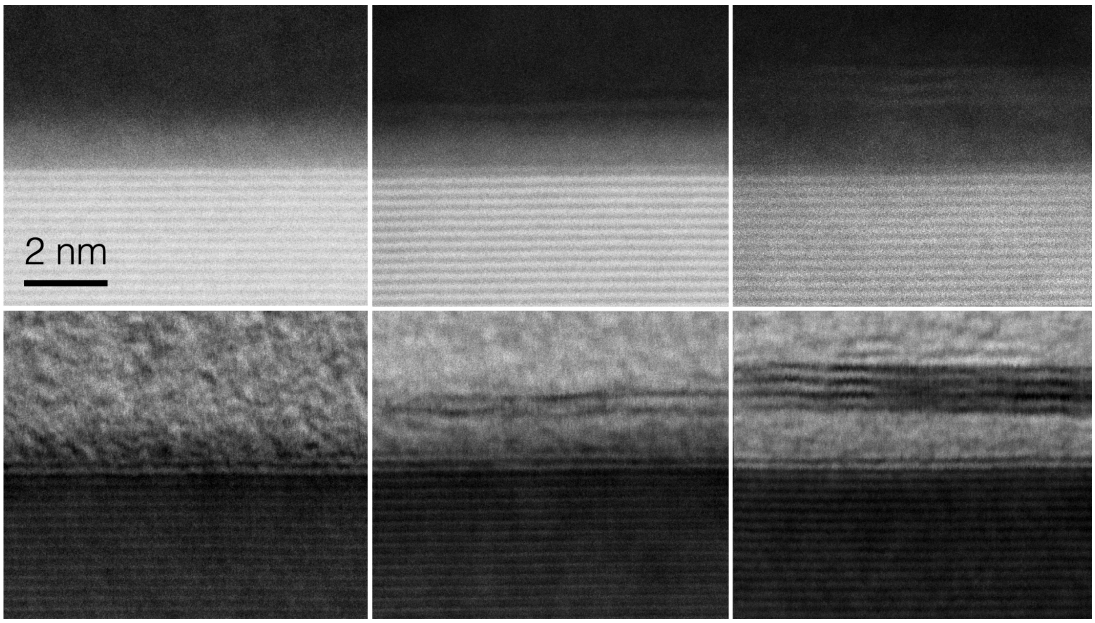

FIG. 2. High-angle annular dark-field (above) and bright-field (below) STEM images at three different areas of the graphene/SiC(000$\bar{1}$) system, showing zero (left), one (center), and three graphene layers (right) on top of an amorphous thin film. The acquisition took place at a 60-keV primary beam energy in order to prevent a beam-induced damage.

AFM tip at different surface positions; hence, it can provide information on the variation in the number of graphene layers at different positions [28]. Interestingly, the regions with the highest phase contrast correspond to areas without wrinkles in the morphological image, i.e., to bare SiC regions, whereas the regions with lower phase contrast correspond to regions with wrinkles in Fig. 1(a). To get a more quantitative information, a histogram of the phase values extracted from Fig. 1(b) is reported in Fig. 1(e). This histogram exhibits three main peaks (indicated by arrows), that can be associated to the bare SiC region (∼36% of the surface) and to regions with a lower and higher number of graphene layers (corresponding to ∼20 and ∼44% of the surface coverage), respectively. However, the exact number of layers cannot be established by the AFM analysis. This information can be provided by the cross-sectional STEM analysis, as shown in the following.

In order to understand the possible reasons for the presence of this structural inhomogeneity, we performed a cross-sectional structural and spectroscopic investigation by means of an aberration-corrected STEM operated at a primary beam energy of 60 keV. Notwithstanding the low operating energy of the microscope (which is well below the knock-on threshold of carbon [29]), we were able to obtain atomic-resolution images as well as EELS acquisitions without damaging the structure. Figure 2 shows three high-angle annular dark-field and bright-field STEM images obtained at different locations of our sample. The common characteristic of all three snapshots is the presence of an amorphous film on top of the SiC substrate, independently from the presence or not of graphene. From the dark-field images as well as from EELS measurements we were able to distinguish this amorphous region from the epoxy glue used for specimen preparation (which can be observed above the interface and graphene layers and has a lower Z contrast with respect to the interface amorphous film). Moreover we note that the epoxy glue at the sample's surface ensured the presence of an undamaged sample underneath its line. Curiously, we found only small variations in the thickness of the amorphous interface film throughout our sample, notwithstanding a variability in the number of the overlying graphene layers from zero to seven. The distance between the first graphene layer and the last SiC bilayer was ∼1.1–1.4 nm, which is indicative of the approximate thickness of the amorphous region. Moreover, in accordance with the AFM measurements, we also found a moderate long-range corrugation of the graphene layers due to stress-relaxation mechanisms. We note here that such corrugation is independent from the problem of graphene detachment during sample preparation at the C-terminated surface [17]. The origin of the constant thickness of the amorphous layer independently from the number of graphene layers could be explained by a growth process that starts from the SiC surface and diffuses toward the bulk. As the SiC surface prior to graphene growth is not perfectly flat, we can expect enhanced sublimation mechanisms in areas where Si coordination is lower than in bulk SiC (e.g., islands, steps, defects, etc.). It is highly probable that such areas are responsible for the bigger number of graphene layers as compared to others with a smaller number.

The interface between the amorphous layer and the SiC substrate also shows some interesting characteristics as the Z contrast of the highest SiC bilayer is lower with respect to underlying bilayers [Figs. 2(b) and 2(c)]. This aspect could be an indication of the process kinetics, where the amorphous layer gradually diffuses toward the bulk of SiC as Si atoms sublimate. Within this scheme, new graphene layers should form below the existing ones as soon as the available C concentration allows it. It should be noted here that a similar growth mechanism has been demonstrated for graphene grown on the Si face of SiC [30]. At the moment it is not clear if the lower Z contrast for the highest SiC bilayer shows simply a

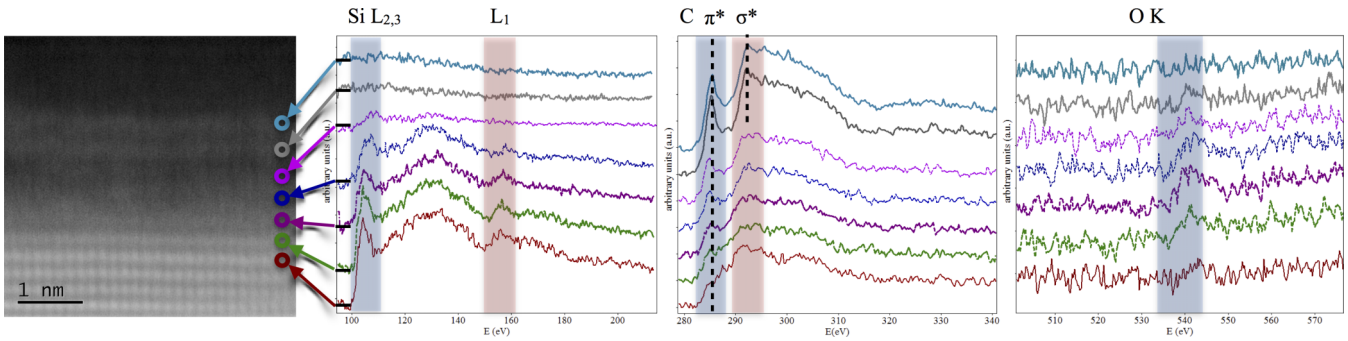

FIG. 3. (Color online) C-K, Si-L and O-K EELS spectra extracted from a two-dimensional spectrum acquired on a SiC terrace. The corresponding high-angle annular dark-field STEM image is shown at the left.

random reduction of the Si concentration or if it can be related to the presence of ordered SiC surface reconstructions [16]. As a final point of the morphological analysis, we underline the first direct imaging of a single layer of graphene grown on the C face of SiC [Fig. 2(b)], which evidences that monolayer samples can indeed grow on the C-terminated surfaces.

IV. CHEMICAL ANALYSIS AND ELECTRONIC STRUCTURE

The chemical features of the graphene/SiC(000$\bar{1}$) interface were studied by means of EELS measurements in a layer-by-layer acquisition [12], starting from the SiC substrate and heading toward graphene. Figure 3 shows the respective results for the Si-$L_{2,3}$, Si-L_1, C-K, and O-K edges. Starting from the C-K edge, we notice the absence of a π^* peak when the electron beam focuses at the SiC substrate. As the beam moves toward the amorphous region we observe the gradual appearance of the characteristic π^* peak at 285.2 eV, which is the signature of $1s$ to π^* electronic transitions. When such a peak is not accompanied by a sharp σ^* peak at 291.5 eV it gives strong evidence that the C contained in this area has amorphous characteristics. When the electron beam focuses on the first and the second graphene layers we observe the presence of sharp π^* and σ^* peaks that denote a purely sp^2 hybridized graphitic carbon. An important issue is the slight shift of the π^* peak toward lower energies in the amorphous region, which could indicate defect states or chemical bonding with other species. Previous studies have claimed the presence of oxygen at the graphene/SiC(000$\bar{1}$) system [5,31]. In order to verify this hypothesis, we controlled for an O-K edge signal during EELS acquisition, which showed the presence of a very low oxygen concentration confined within the amorphous region. It is still unclear if such oxidation takes place during the growth process or if it is the result of postgrowth contamination. We note, however, that no similar oxidation takes place when growing graphene on the Si face under similar conditions, as well as that annealing temperatures are too high for the persistent presence of an oxide during growth. Further study is necessary in order to clarify this issue.

By observing the EELS spectra related to Si-L peaks we can deduce some interesting characteristics about the presence of Si in our samples. We initially note a prominent Si-L_1 peak in the SiC bulk at 155 eV which is indicative of sp^3 hybridization, as expected for the SiC bulk. The intensity of this peak gradually drops when moving toward the amorphous area and vanishes when focusing the electron beam on the two graphene layers. Similar characteristics are visible for the Si-$L_{2,3}$ peak, although noise levels are prohibiting for a precise signal background subtraction.

In order to quantify the relative concentrations of C and Si in our samples we have integrated the intensities of the C-K and Si-L EELS spectra, taken across the whole HAADF STEM image of Fig. 4, using a pixel step size of 0.6 Å and an exposure time of 20 ms for each pixel. All the spectra were corrected for the effects of energy drift and plural scattering using the simultaneously acquired low-loss spectra. As expected, within the SiC bulk, both C and Si have the same areal density as the atomic concentration is equal. A detachment from this trend can be observed when the electron beam focuses at the last SiC bilayer and moves toward the amorphous region. There, a gradual increase in the C areal density is accompanied by a respective decrease of the Si density. The formation of graphene layers takes place as soon as the Si concentration vanishes. These results show that the amorphous region is highly inhomogeneous in its Si concentration and also indicate that such partial sublimation of Si is the reason for the amorphization (and not graphitization) of the interface area.

V. *AB INITIO* CALCULATIONS

The experimental analysis shows a higher degree of interface disorder for epitaxial graphene on the C face of

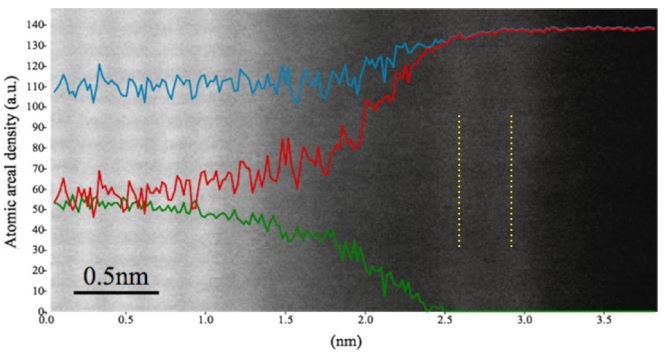

FIG. 4. (Color online) Atomic areal density in arbitrary units for C (red line) and Si (green line), acquired by integrating the C-K and Si-L EELS peaks while focusing the electron beam from the substrate toward graphene. The blue line indicates the sum.

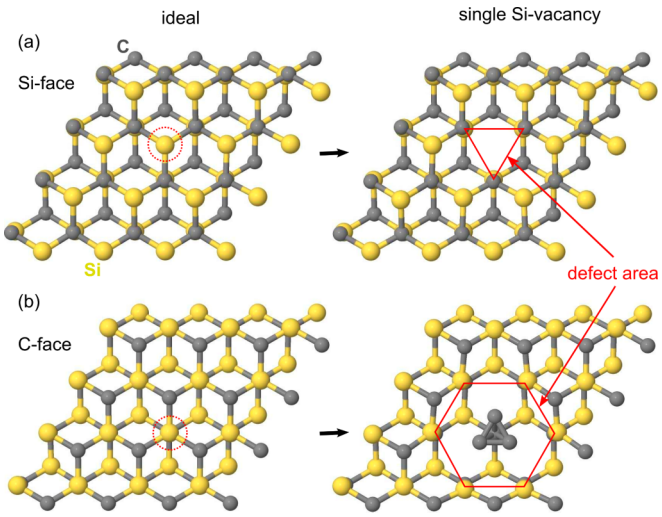

FIG. 5. (Color online) Structural modifications on the two SiC{0001} surfaces when a single Si vacancy is present: (a) SiC(0001) surface and (b) SiC(000$\bar{1}$) surface.

SiC as compared to the well-characterized buffer layer of the Si face. However the experiment is not capable of resolving the structural alterations that emerge during the sublimation process, nor of justifying the growth differences between the two SiC{0001} surfaces. To this end we performed DFT calculations in order to understand the morphological modifications on the two {0001} planes when Si vacancies are created. Figure 5 shows calculation results based on a simple Si-sublimation model with the creation of single Si vacancies on the surface (considering the entire top SiC bilayer as the surface). We point out that the starting point of the simulation is different for the Si and the C face, as the topmost Si atom has a coordination number $n_c = 3$ at the Si face and $n_c = 4$ at the C face. By itself, this purely geometrical fact should facilitate the formation of Si vacancies on the Si face rather than the C one. Indeed, our calculations showed that the energy requirement for the formation of a Si vacancy is lower by 2.25 eV at the ideal Si-terminated surface with respect to the C-terminated surface. However, the calculation revealed a completely different picture when considering the structural modifications of the material: The Si vacancy on the Si face hardly perturbs the structural order of the neighboring atoms [Fig. 5(a)]. In particular, the three neighboring C atoms are marginally displaced away from the vacancy site, adjusting their hybridization to a "more" sp^2-type configuration. On the other hand, on the C face, a strong reconstruction around the vacancy site is observed, with the four C neighboring atoms merging in a pyramidal agglomerate that substitutes the missing Si, while breaking their bonds with six neighboring Si atoms [Fig. 5(b)]. Such bond breaking extends the defect area to second-neighbor Si atoms, which all acquire a coordination number $n_c = 3$, becoming preferential sites for further Si sublimation. Our calculations emphasize two important features of the sublimations process: (1) Qualitatively the sublimation of Si strongly increases the level of disorder on the C face as compared to the Si face and (2) sublimation should be relatively uniform at the Si face while strongly localized around defect sites and nonplanar areas at the C face. These two aspects should be at the origin of the different interface morphologies and graphene coverages obtained during the experiment.

VI. DISCUSSION

Notwithstanding that the graphene/SiC(000$\bar{1}$) interface can be sensitive to growth conditions [6,16,32], our study shows that under thermal annealing at high temperatures ($T = 1900\,^{\circ}$C here) in a high-pressure Ar environment (1) a thin C/Si amorphous layer forms at the interface between graphene and SiC; (2) the thickness of this layer does not depend on the number of the overlying graphene layers; (3) the amorphous layer is inhomogeneous, as its Si concentration gradually decreases while approaching the surface; (4) this layer is partially oxidized; and (5) the presence of this layer totally decouples the two parts of the heterostructure (as its thickness is bigger than the range of chemical bonds between atoms of the first graphene layer and the last SiC bilayer) and, hence, suppresses epitaxy. This last aspect can be also confirmed by the absence of a clear in-plane lattice spacing for the graphene layers in any of our STEM images and indicates that graphene has a rotational stacking which is independent from the substrate (in contrast with what happens on the Si face). Further work is necessary for the determination of the structural/chemical properties of the amorphous/disordered layer at different growth temperatures as well as for the precise characterization of its oxidation characteristics.

By comparing the interface properties of C-terminated SiC with those of its Si-face counterpart, we find some interesting similarities along with subtle differences. In both cases an interface structure is present; however, at the Si face this is composed only of C [11] and has a well-defined honeycomb geometry [10]. On the other hand, the C-terminated amorphous layer shows chemical signatures of three elements (C, Si, and O) and it is significantly thicker. Moreover, in both cases the first graphene layer that grows on top of the interface layer has sp^2-type characteristics. The presence of disorder on the C-face interface layer in conjunction with the lower temperatures needed in order to have a comparable graphene coverage on the entire wafer may be indicative of a faster sublimation process. This indication could be consistent with a facilitated Si out-diffusion through an amorphous interface with respect to the diffusion through the ordered buffer layer on the Si face. We note that in order to create a single graphene layer (or a single buffer layer) Si needs to sublimate from at least three bilayers of SiC, which, in turn, have a comparable thickness with the amorphous interface layer. Finally, the stronger reactivity of the amorphous interface could explain the observed O incorporation during or after the sublimation process.

In conclusion, in this study we have presented results for graphene grown on the C face of SiC using high-resolution STEM/EELS and AFM measurements, accompanied by DFT calculations. Our analysis showed the presence of an inhomogeneous, partially oxidized C/Si amorphous layer at the graphene/SiC interface which should strongly suppress epitaxy in this system. Our results are relevant for the better understanding of graphene formation on the SiC(000$\bar{1}$) surface and its potential use in devices and applications.

ACKNOWLEDGMENTS

This work has been supported by the Ministero dell'Istruzione, dell'Università e della Ricerca under project Beyond-Nano (Grant No. PON a3_00363) and the European Science Foundation under the EUROCORES Program Euro-GRAPHENE CRP GRAPHIC-RF.

[1] K. V. Emtsev, A. Bostwick, K. Horn, J. Jobst, G. L. Kellogg, L. Ley, J. L. McChesney, T. Ohta, S. A. Reshanov, J. Röhrl, E. Rotenberg, A. K. Schmid, D. Waldmann, H. B. Weber, and T. Seyller, Nat. Mater. **8**, 203 (2009).

[2] V. Darakchieva, A. Boosalis, A. A. Zakharov, T. Hofmann, M. Schubert, T. E. Tiwald, T. Iakimov, R. Vasiliauskas, and R. Yakimova, Appl. Phys. Lett. **102**, 213116 (2013).

[3] C. Virojanadara, M. Syväjarvi, R. Yakimova, L. I. Johansson, A. A. Zakharov, and T. Balasubramanian, Phys. Rev. B **78**, 245403 (2008).

[4] D. K. Gaskill, G. Jernigan, P. Campbell, J. L. Tedesco, J. Culbertson, B. VanMil, R. L. Myers-Ward, C. Eddy, J. Moon, D. Curtis *et al.*, ECS Trans. **19**, 117 (2009).

[5] Luxmi, N. Srivastava, G. He, R. M. Feenstra, and P. J. Fisher, Phys. Rev. B **82**, 235406 (2010).

[6] L. I. Johansson, S. Watcharinyanon, A. A. Zakharov, T. Iakimov, R. Yakimova, and C. Virojanadara, Phys. Rev. B **84**, 125405 (2011).

[7] X. Wu, Y. Hu, M. Ruan, N. K. Madiomanana, J. Hankinson, M. Sprinkle, C. Berger, and W. A. de Heer, Appl. Phys. Lett. **95**, 223108 (2009).

[8] J. L. Tedesco, B. L. Vanmil, R. L. Myers-Ward, J. M. McCrate, S. A. Kitt, P. M. Campbell, G. G. Jernigan, J. C. Culbertson, C. R. Eddy, and D. K. Gaskill, Appl. Phys. Lett. **95**, 122102 (2009).

[9] K. V. Emtsev, F. Speck, T. Seyller, L. Ley, and J. D. Riley, Phys. Rev. B **77**, 155303 (2008).

[10] S. Goler, C. Coletti, V. Piazza, P. Pingue, F. Colangelo, V. Pellegrini, K. V. Emtsev, S. Forti, U. Starke, F. Beltram *et al.*, Carbon **51**, 249 (2013).

[11] J. D. Emery, B. Detlefs, H. J. Karmel, L. O. Nyakiti, D. K. Gaskill, M. C. Hersam, J. Zegenhagen, and M. J. Bedzyk, Phys. Rev. Lett. **111**, 215501 (2013).

[12] G. Nicotra, Q. M. Ramasse, I. Deretzis, A. La Magna, C. Spinella, and F. Giannazzo, ACS Nano **7**, 3045 (2013).

[13] S. Kim, J. Ihm, H. J. Choi, and Y.-W. Son, Phys. Rev. Lett. **100**, 176802 (2008).

[14] I. Deretzis and A. La Magna, Phys. Rev. B **84**, 235426 (2011).

[15] A. J. M. Giesbers, P. Procházka, and C. F. J. Flipse, Phys. Rev. B **87**, 195405 (2013).

[16] F. Hiebel, P. Mallet, F. Varchon, L. Magaud, and J.-Y. Veuillen, Phys. Rev. B **78**, 153412 (2008).

[17] W. Norimatsu and M. Kusunoki, J. Phys. D **47**, 094017 (2014).

[18] J. Borysiuk, R. Bożek, K. Grodecki, A. Wysmołek, W. Strupiński, R. StePniewski, and J. M. Baranowski, J. Appl. Phys. **108**, 013518 (2010).

[19] J. Borysiuk, J. Sołtys, R. Bożek, J. Piechota, S. Krukowski, W. Strupiński, J. M. Baranowski, and R. Stępniewski, Phys. Rev. B **85**, 045426 (2012).

[20] R. Colby, M. L. Bolen, M. A. Capano, and E. A. Stach, Appl. Phys. Lett. **99**, 101904 (2011).

[21] X. Weng, J. A. Robinson, K. Trumbull, R. Cavalero, M. A. Fanton, and D. Snyder, Appl. Phys. Lett. **100**, 031904 (2012).

[22] K. Kimura, K. Shoji, Y. Yamamoto, W. Norimatsu, and M. Kusunoki, Phys. Rev. B **87**, 075431 (2013).

[23] O. L. Krivanek, N. Dellby, M. F. Murfitt, M. F. Chisholm, T. J. Pennycook, K. Suenaga, and V. Nicolosi, Ultramicroscopy **110**, 935 (2010).

[24] J. M. Soler, E. Artacho, J. D. Gale, A. García, J. Junquera, P. Ordejón, and D. Sánchez-Portal, J. Phys.: Condens. Matter **14**, 2745 (2002).

[25] J. P. Perdew and A. Zunger, Phys. Rev. B **23**, 5048 (1981).

[26] N. Troullier and J. L. Martins, Phys. Rev. B **43**, 1993 (1991).

[27] H. J. Monkhorst and J. D. Pack, Phys. Rev. B **13**, 5188 (1976).

[28] C. Vecchio, S. Sonde, C. Bongiorno, M. Rambach, R. Yakimova, V. Raineri, and F. Giannazzo, Nano. Res. Lett. **6**, 269 (2011).

[29] O. L. Krivanek, M. F. Chisholm, V. Nicolosi, T. J. Pennycook, G. J. Corbin, N. Dellby, M. F. Murfitt, C. S. Own, Z. S. Szilagyi, M. P. Oxley *et al.*, Nature (London) **464**, 571 (2010).

[30] H. Huang, W. Chen, S. Chen, and A. T. S. Wee, ACS Nano **2**, 2513 (2008).

[31] C. E. Giusca, S. J. Spencer, A. G. Shard, R. Yakimova, and O. Kazakova, Carbon **69**, 221 (2014).

[32] N. Srivastava, G. He, Luxmi, and R. M. Feenstra, Phys. Rev. B **85**, 041404(R) (2012).